Experimental results of a 1D passive magnetic spring approaching quasi-zero stiffness and using active skyhook damping

William S. P. Robertson, Ben Cazzolato, and Anthony Zander

School of Mechanical Engineering, The University of Adelaide, Australia

ABSTRACT

The use of permanent magnets has been investigated in recent years to provide load bearing forces for vibration isolation. Using two pairs of magnets in both repulsion and attraction, it is possible to generate a force-displacement characteristic that has an inflection point at zero stiffness, known as the quasi-zero stiffness location. Since vibration isolation performance is known to improve with lower resonance frequencies and therefore isolator stiffnesses, the quasi-zero stiffness location is considered the point at which vibration isolation is best achieved. However, since this location is only marginally stable, for passive operation it is only possible in practice for the equilibrium position of the system to asymptotically approach the quasi-zero stiffness point. The proximity to this point that can be achieved depends on the loads to be borne and the amplitude of vibration to be isolated. In previous works, this particular magnetic system has seen theoretical treatment. A prototype of the magnetic system will be presented that uses magnet pairs mounted on a rigid lever arm to constrain their motion to a single degree of freedom. Experimental results are presented that demonstrate the quasi-zero stiffness behaviour of the practical system. Finally, a novel electromagnetic actuator is incorporated into the design to attenuate the resonance peak via active skyhook damping using accelerometer measurements. The limits of this feedback are shown to be caused by the filter poles of the accelerometers used to measure the vibration.

INTRODUCTION

Vibration isolation of sensitive equipment involves mounting with as low a stiffness as possible to reduce the resonance frequency of the system. Several approaches have been suggested for adding negative stiffness elements in series with a vibration mount in order to reduce the resonance frequency while maintaining its load-bearing ability, including flexible members (Tarnai 2003; Cella et al. 2005; Lee, Goverdovskiy, and Temnikov 2007), 'buckling' springs (Molyneux 1957; Alabuzhev et al. 1989; Carrella, Brennan, and Waters 2007; Carrella et al. 2009), and attracting pairs of magnets (Carrella et al. 2008; Robertson et al. 2009; Robertson et al. 2006; Robertson, Cazzolato, and Zander 2007; Zhu et al. 2011).

While in theory such systems are refered to as having 'quasi–zero stiffness', this term is slightly misleading as the position of dynamic zero stiffness is only marginally stable and the system cannot stably operate at this point. Linear control systems can be used to stabilise such a system, but the additional dynamics of the controller will have their own influence on the propagated vibration disturbance. For stable operation, the nominal operating position of the system must be chosen sufficiently far away such that the maximum excursion from equilibrium remains within the stability region (Robertson et al. 2009). In this case, the system will have a non-zero but small positive stiffness; further improvement to the vibration isolation properties of the system can be achieved using standard active vibration feedback control.

This paper documents a set of experiments that were conceived to demonstrate these ideas. A single degree of freedom system was designed using one pair of magnets in repulsion for load bearing and one pair in attraction for stiffness reduction (Fig. 1). The system was tuned to achieve a minimal resonance frequency and active vibration isolation used to improve the transmissibility for vibration isolation.

DESCRIPTION OF APPARATUS

The experimental apparatus that was designed and built as part of this project is shown as a schematic in Fig. 1 and as a photograph in Fig. 2. Physical parameters of the design are shown in Table 1.

The rig consists of an arrangement of magnets, of which two are fixed to the frame; 'floating' magnets are supported by these of which one is situated below to apply a repulsive force (positive stiffness) and the other is situated above to apply an attractive force (negative stiffness). The physical location of the fixed magnets may be moved vertically in order to vary the respective amounts of positive and negative stiffness.

The magnet system is designed to investigate the dynamics in the vertical displacement direction; having stability in this direction implies instability in the horizontal direction (Bassani 2006). In order to remain stable, the magnets require a physical constraint, achieved by placing the floating magnets at the end of a long pinned rigid beam. Small rotations of this beam can be assumed to correspond to largely vertical displacements of the end magnets.

Table 1. Physical properties of the experimental rig.

Rig height	H	209 mm
Beam mass	m_b	266 g [a]
Beam length	L_b	320 mm
Beam height	h_b	25 mm
Beam width	w_b	40 mm
Beam thickness	t_b	2 mm
Beam vertical offset	o_b	82 mm
Magnet support height	h_m	105 mm
Magnet support lever arm	L_m	300 mm
Magnet support mass	m_m	87 g
Magnets height	h	9.5 mm
Magnets diameter	$2R_m$	12.7 mm
Magnets remanence	B_r	1.3 T
Lower fixed magnet origin	o_m	44 mm
Upper fixed magnet origin	o_n	30 mm plus offset [b]
Sensor height	h_s	85 mm
Sensor horizontal offset	L_s	252 mm
Sensor displacement measurement	x_s	43 mm–53 mm

[a] Mass of the accelerometer is accounted for in this value.
[b] Offset varied to adjust the amount of added negative stiffness.

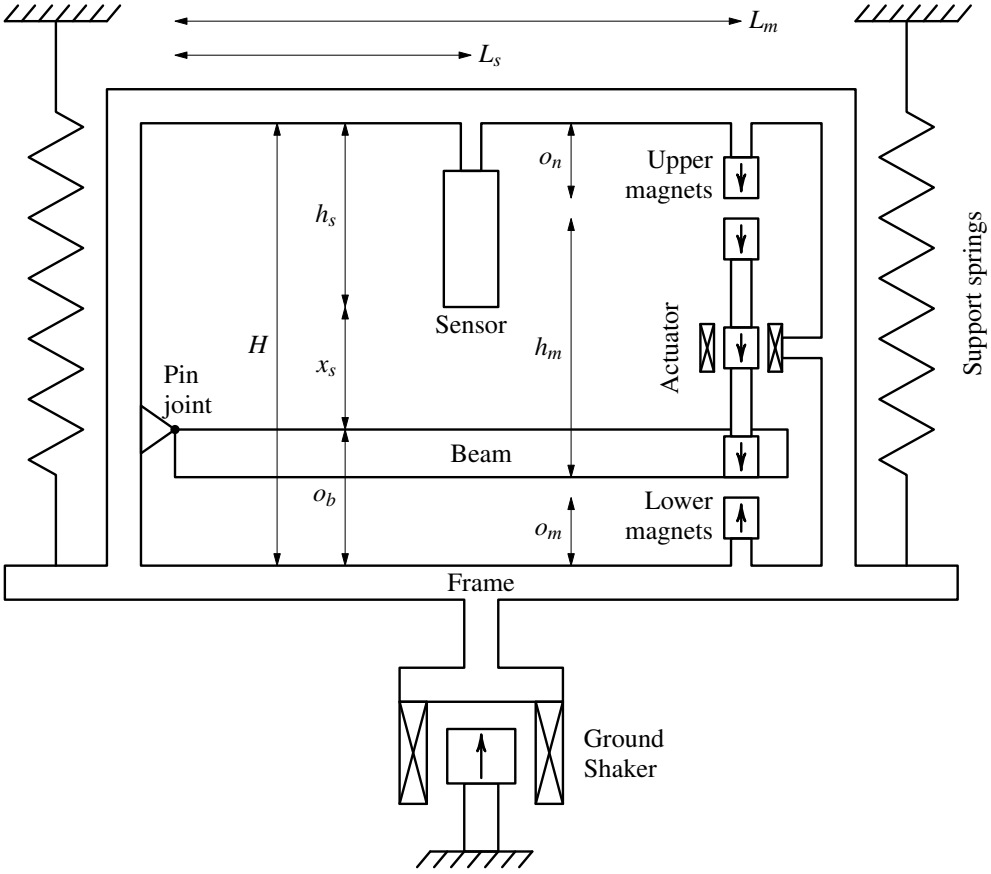

Figure 1. Schematic of the experimental rig (not to scale). Position shown is the marginally stable configuration with equal gap between the lower and upper pairs of magnets.

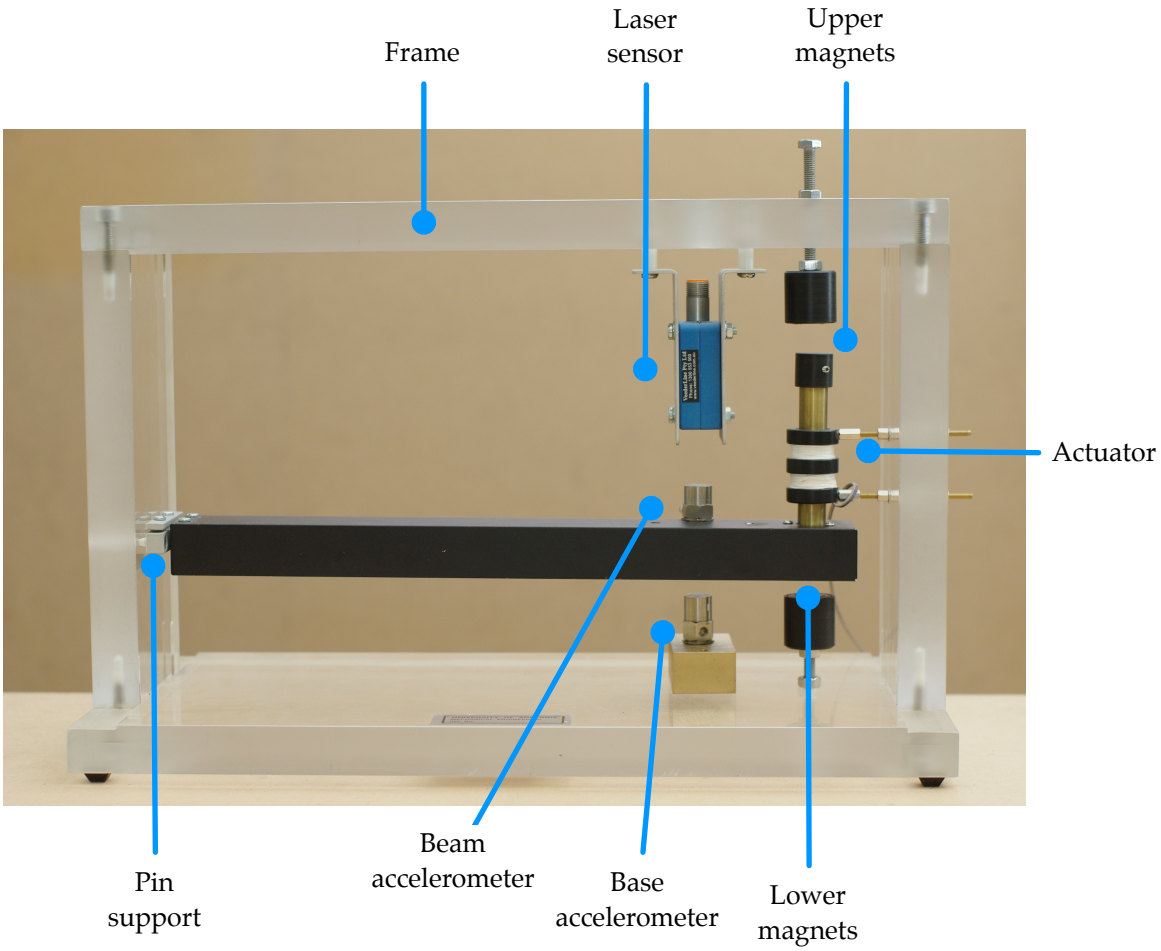

Figure 2. Photo of the experimental apparatus. Base shaker is not shown.

The beam itself was chosen as a hollow rectangular section in order to minimise weight and maximise stiffness; it is assumed to be a rigid body for the purposes of these experiments (especially at the low vibrational frequencies under investigation).

The pin support was constructed by clamping the beam to a thin piece of flexible plastic which was clamped to the frame. The use of a flexural element was chosen to avoid static friction that would be present in a bearing or hinge joint. The stiffness of this plastic can be assumed to be negligible as it played no part in the load bearing of the beam.

Electromagnetic actuator

A dual-coil electromagnetic arrangement was custom-built for the actuator for the experimental apparatus. A schematic of the dual-coil system is shown in Fig. 3 with parameters in Table 2. The coil was designed to have an impedance of 8 Ω, from which the outer radius of the coil was calculated given a certain wire diameter and resistance (Robertson, Cazzolato, and Zander 2012).

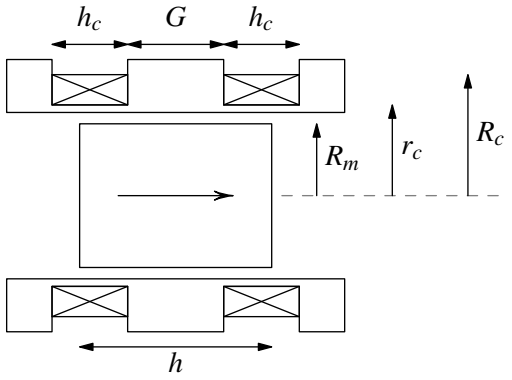

Figure 3. Schematic of the dual-coil electromagnet built for the experimental apparatus. (Not to scale.)

Table 2. Dual-coil electromagnet parameters.

Magnet radius	R_m	6.4 mm
Magnet height	h	9.5 mm
Coil height	h_c	7 mm
Coil inner radius	r_c	10 mm
Coil outer radius	R_c	10.7 mm
Coil gap	G	7 mm
Turns (approx.)		105
Former inner radius		14.2 mm

The dimensions of the coil were chosen to ensure sufficient force over the displacement range expected from the system. The force imparted by the coil remains within 10% of maximum over a displacement range of around ±2 mm, which is acceptable for the purposes of the design.

Displacement and acceleration sensors

The sensor purchased for the experimental apparatus was a Wenglor 05 MGV 80 opto-electronic sensor, which uses a laser to measure distance over a range of 10 mm.

For the beam, a Brüel and Kjær 4367 accelerometer was used to measure the 'output' signal; for the base, a 4332 accelerometer measured the 'input' signal of the system. The accelerometers were used with Brüel and Kjær 2635 charge amplifiers set to appropriate gain values for the input signals. The signals were low-pass filtered at 50 Hz to avoid aliasing effects using a Krohn-Hite Model 3362 digital filter (using a 4-pole Butterworth filter).

For open loop measurements, these accelerometers were used to measure acceleration directly; for closed loop control, the charge amplifier was used to integrate the measured signals to estimate the velocities. The high-pass filter in the charge amplifiers used a 0.1 Hz cut-on frequency when measuring acceleration and 1 Hz for velocity. The higher frequency is necessary for velocity to avoid drift due to accumulation of errors in the integrator circuit.

Translational effects of the rotating beam

Three moving magnets were required in the system: one at the main end of the motional beam to be repelled for positive stiffness by the fixed lower magnet; a second to be used with electromagnetic coil for control forces; and the third to be attracted for negative stiffness by the fixed upper magnet.

The beam added a horizontal constraint to the system for stability. As the beam rotates, the magnets move predominantly in the vertical direction; there is still some horizontal motion, however, and the area restricted by the electromagnetic coil requires attention to ensure that there is no contact between the moving magnet and the fixed coil. However, the smaller the air gap between the coil and the magnet, and thus the smaller the inner radius of the coil, the greater the forces imparted by the coil on the magnet, so the smaller the tolerance the better.

The actual clearance between the outer radius of the brass cylinder holding the magnets and the inner radius of the coil former was 0.35 mm. This tolerance was judged to be small enough to allow a surrounding coil without having a significantly diminished force characteristic from the air gap required to avoid contact. It should be noted that this tolerance caused a degree of inconvenience since the attachment and positioning of the coil required careful alignment in order to allow free movement of the cylinder holding the magnets.

EXPERIMENTAL RESULTS

A number of measurements were performed using the experimental apparatus; in the sections following, measured data is presented for: magnet gap versus beam displacement; open loop frequency responses for a range of magnet gaps; and, velocity feedback in a single configuration.

Static displacement measurements

The upper magnet's position was varied until the limit of stability was reached. The lower fixed magnet was kept fixed, which means that the position of quasi–zero stiffness was changing; with counter-threaded mounts for the upper and lower magnets, they could be adjusted in parallel to achieve a fixed quasi–zero stiffness location.

As the upper magnet placement was lowered, the rest position of the beam moved closer to the quasi–zero stiffness position (as more force was supported by the upper magnet). This relationship is shown in Fig. 4b. The normalised magnet gap g is used in the following sections to represent the varied configuration of the spring in the experiments, defined as $g = o_g/h$, where o_g is the magnet gap at quasi–zero stiffness and h is the height of the magnets. From the geometry of the rig, the position of the upper magnet was used to calculate the gap between the magnets at quasi–zero stiffness:

$$o_g(o_n) = \tfrac{1}{2}\left[H - o_m - o_n - h_m\right] + h - h_\varepsilon, \qquad (1)$$

where geometrical properties are described in Table 1 and $h_\varepsilon = 2.5$ mm is an extra clearance to account for space taken up by the thicknesses of the magnet mounting. The height of the quasi–zero stiffness location itself, o_q, is given by

$$o_q(o_n) = \tfrac{1}{2}\left[H - o_m + o_n\right]. \qquad (2)$$

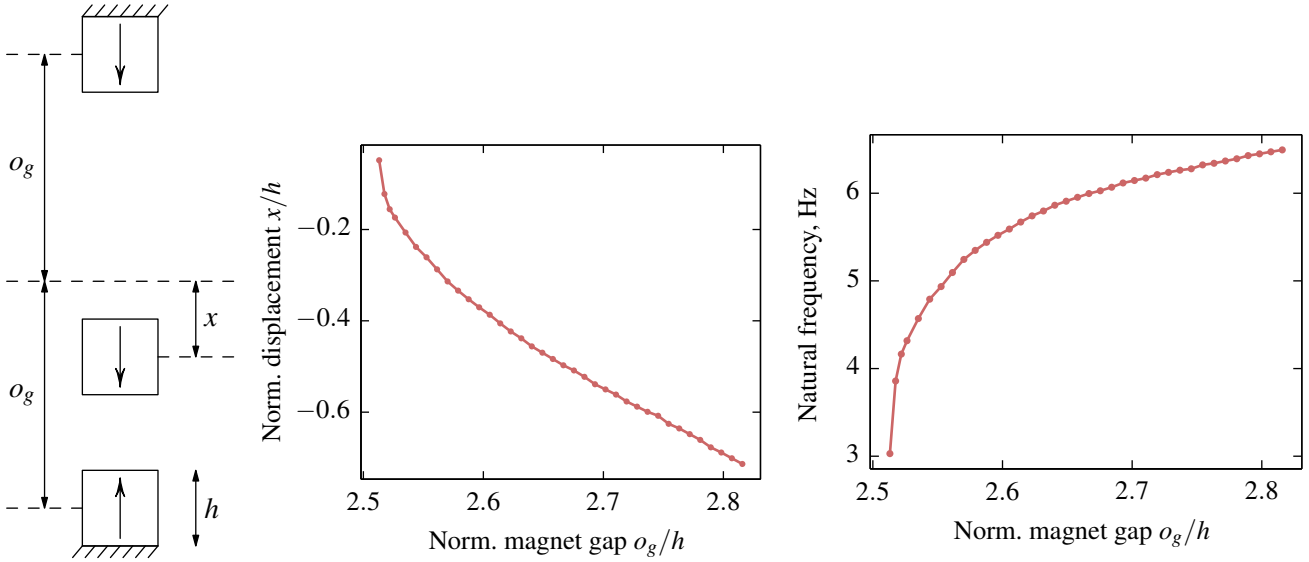

(a) Geometry. **(b)** Measured equilibrium position as the magnet position varies. **(c)** Expected natural frequency as the magnet position varies.

Figure 4. Measured rest position of the system as the magnet position varies. For simplicity, only a single floating magnet is shown here.

The measured output of the sensor x_s was used to infer a magnet displacement, x, (referenced from the quasi–zero stiffness position) with the following relationships. Firstly, the rotational origin of the beam was used as a vertical reference point, and the displacement of the beam x_b at the laser sensor location calculated as

$$x_b(x_s) = H - o_b - h_s - x_s, \tag{3}$$

which can be extrapolated using the respective lever arms to calculate the resultant vertical displacement of the moving magnets with respect to the beam origin with

$$x_p(x_b) = x_b \frac{L_m}{L_s}. \tag{4}$$

This moving magnet displacement can be written with respect to the origin of the frame of the rig with

$$x_m(x_p) = o_b + x_p - h_b + t_b + \tfrac{1}{2}h_m. \tag{5}$$

Accordingly, the displacement of the system x from the quasi–zero stiffness location is given by

$$x(x_s, o_n) = x_m - o_q. \tag{6}$$

The displacements between the centres of each magnet in the interacting pairs can be similarly calculated based on the displacement of the moving magnet assembly x_m. With respect to the frame origin, the magnet centres for the base magnet m_1, upper magnet m_2, lower moving magnet m_3, and upper moving magnet m_4 are

$$m_1 = o_m - h_\varepsilon - \tfrac{1}{2}h, \tag{7}$$

$$m_2 = H - \left[o_n - h_\varepsilon - \tfrac{1}{2}h\right], \tag{8}$$

$$m_3 = x_m - \tfrac{1}{2}h_m + \tfrac{1}{2}h, \tag{9}$$

$$m_4 = x_m + \tfrac{1}{2}h_m - \tfrac{1}{2}h. \tag{10}$$

Predicted resonance frequencies

From the displacement results shown previously, predicted resonance frequencies can be calculated for this system as a function of magnet gap. The expected magnetic forces F due to the measured displacements were calculated using the theory for coaxial cylindrical magnets (Robertson, Cazzolato, and Zander 2011) based on magnet centre displacements $m_3 - m_1$ and $m_2 - m_4$. Numerical differentiation was used to calculate the stiffnesses k at these displacements, and the natural frequency at each location calculated with $\omega_n = \sqrt{k/m_{eq}}$ where $m_{eq} = F/g$ is the equivalent mass borne by the static force F. With parameters as specified, the expected natural frequency versus magnet gap results are shown in Fig. 4c.

Open loop dynamic measurements

As the position of the upper magnet is varied, the amount of negative stiffness added to the system changes. This predominantly affects the rest position and the resonance frequency, along with small changes in damping. Frequency response measurements were taken at a number of discrete locations of the upper fixed magnet to observe the changes in dynamics as the rest position of the system approached the quasi–zero stiffness position.

The parameters used to perform the spectral analysis for each measurement are shown in Table 3. Due to the low damping and low resonance frequency of the system, very long sample times were required to achieve results with enough frequency resolution and sufficient coherence to characterise the response. A high sample rate (1000 Hz) was chosen to reduce the possibility of controller time delays influencing the feedback control.

Table 3. Parameters used in the signal and spectrum analysis for the experimental measurements.

Sample rate	1000 Hz
FFT points	2^{16}
Sample time	≈17.5 min
Average overlap	0.75
Number of non-overlapping averages	16

Open loop measurements were taken both with and without the electromagnetic actuator connected (wired as both a short circuit and an open circuit). In the closed circuit configuration, the coil adds damping via induced eddy currents from the moving magnet. As an open circuit, the coil has no effect on the dynamics of the system.

Open loop measurements without the coil connected are shown in Fig. 5a and measurements taken with the coil (that is, with

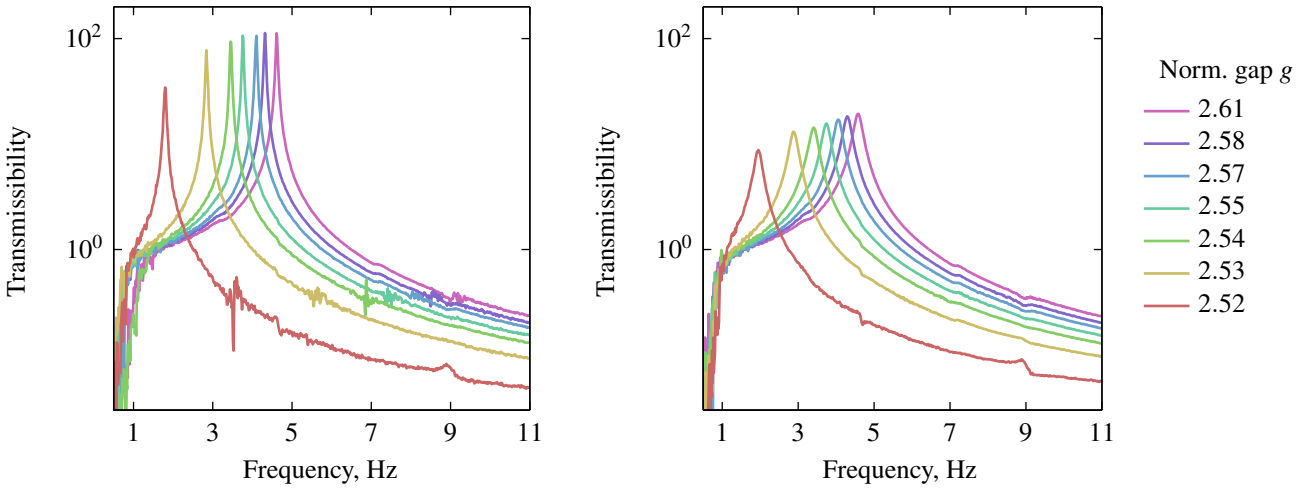

(a) Open circuit coil; no additional damping is added to the system.

(b) Closed circuit coil. The coil adds damping to the system, which can be seen by the reduction in height of the resonant peaks in comparison to Fig. 5a.

Figure 5. Open loop measurements with the electromagnetic coil connected in an open and closed circuit as a function of normalised gap g.

added damping) are shown in Fig. 5b. For both of these results, the transmissibility T shown is the transfer function between the accelerometer measurements of the base and magnet-supported beam:[1]

$$T = \frac{P_{mb}}{P_{bb}}, \tag{11}$$

where P_{bb} is the power spectral density of the accelerometer measurements of the base, and P_{mb} is the cross power spectral density of the magnet and base accelerometer measurements.

Analysis of the open loop data

From the measurements shown in the previous section, data fitting of the frequency response functions was used to extract a linear model of the system in each configuration. While more sophisticated techniques are possible (Chen, Liu, and Lai 2009), fitting the data to a known exact frequency response function yielded acceptable results in this case since the linear model is relatively simple.

The model used to fit the data was a single degree of freedom vibration isolation system in terms of the natural frequency, $\omega_n = \sqrt{k/m}$, and damping ratio $\zeta = b/(2\sqrt{km})$:

$$T(i\omega) = \frac{2i\zeta\omega\omega_n + \omega_n^2}{-\omega^2 + 2i\zeta\omega\omega_n + \omega_n^2}, \tag{12}$$

where ω is the frequency at which to calculate the transmissibility $T(i\omega)$. The data was fit[2] to Eq. (12) between $\frac{1}{2}\omega_n \leq \omega \leq 2\omega_n$, with well-fit transmissibility around the resonance peak at each measurement taken. Due to the influence of unmodelled dynamics in the system, the model starts to deviate from the measured data at higher frequencies. The natural frequencies and damping ratios calculated from this curve fitting are shown in Fig. 6. Comparing the results with the coil circuit open and closed, the resonance frequencies remained constant but the damping ratios changed. With the actuator connected, movement of the actuator magnet caused eddy currents to be induced in the coil, adding damping to the system.

The curve of the measured resonance frequencies (Fig. 6a) follows the same trend as the predicted natural frequencies (redrawn from Fig. 4c). However, their magnitudes are not well

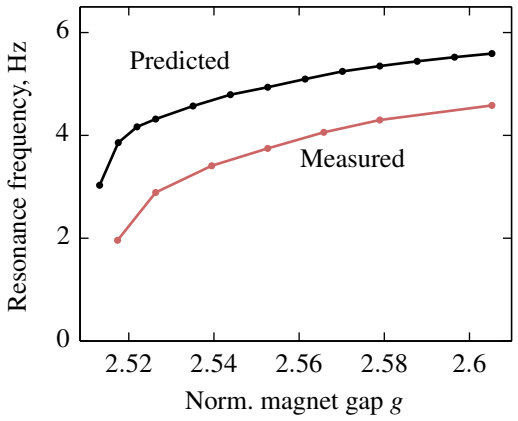

(a) Model-derived resonance frequencies shown with predicted values.

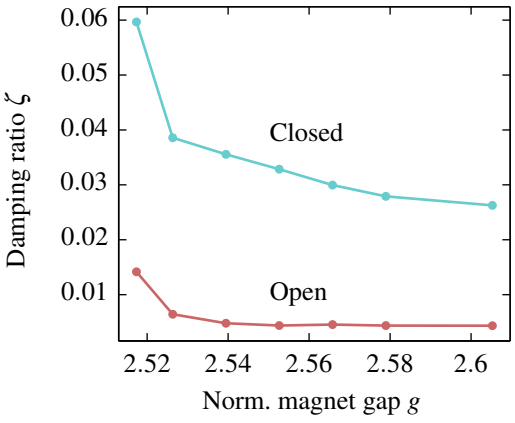

(b) Model-derived damping ratios.

Figure 6. Analysed results from fitting the open loop measurements to the isolator model of Eq. (12).

[1] Calculated with Matlab's `tfestimate` command.
[2] Using Matlab's `fminsearch`.

matched. As the system approaches the quasi–zero stiffness position, even small changes in alignment and physical tolerances have significant effects on the calculated instability region; as seen in the low end of the quasi-static measurements, Fig. 4c, a fraction of a millimetre change in the position of the top magnet can change the natural frequency by 25%. Associatively, with larger magnet gaps the discrepancy becomes lower. Therefore, the discrepancy seen between theoretical and measured results should be expected.

The resonance frequency of the system was unaffected by the presence of the electromagnetic coil (which can also be observed by comparing Figs 5a and 5b) but the damping was increased significantly when the coil circuit was closed.

Observed nonlinear behaviour

The dynamics shown in the undamped case are more nonlinear than the damped case; this is due to the greater displacements experienced by the beam moving the magnets through greater ranges of stiffness variation. When the transmissibility is calculated as the transfer function between the input and output signals, the system is assumed to be linear and nonlinearities are rejected by the ratio of the cross-spectrum and power-spectrum terms in Eq. (11). A different result can be shown by instead calculating the transmissibility via a ratio of the individual power spectra of the magnet and base:

$$T = \sqrt{P_{mm}/P_{bb}}, \tag{13}$$

In this case, any nonlinearities in the signals are retained in the final result.

The transmissibility calculated with this method is shown in Fig. 7 for the coil in an open circuit (that is, low damping). In this case, there are significant nonlinearities present in the data, seen by a clear peak in each spectrum at close to twice the 'linear' resonance frequency. When the coil is connected and the damping present in the system increased, these nonlinearities are no longer seen (the results are indistinguishable to those shown in Fig. 5b). The reduced nonlinearity with increased damping is consistent with the work of other researchers (Jazar et al. 2006).

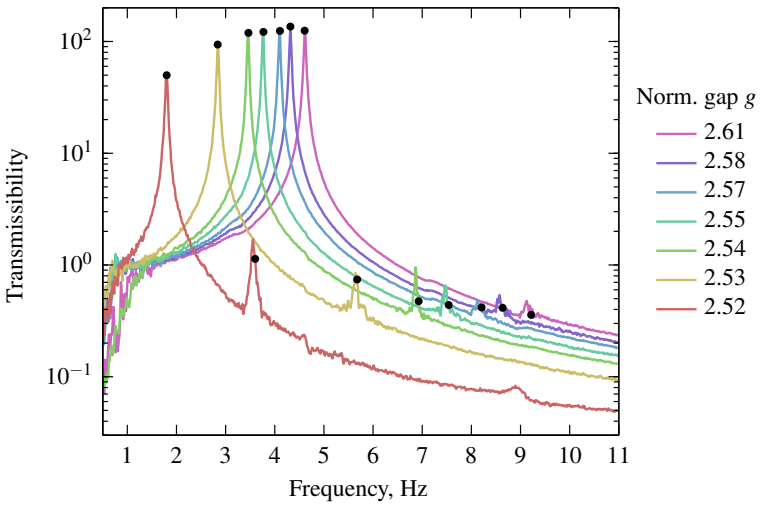

Figure 7. Open loop measurements without the coil connected; the transmissibility is calculated with Eq. (13). Black markers show resonance frequencies and the points at twice each resonance frequency, indicating the nonlinear behaviour.

Closed loop velocity feedback dynamic measurements

In this section, results are shown using closed loop feedback control to improve the vibration isolation characteristics of the system. For this experiment, the rest position of the spring was chosen to achieve an arbitrary low resonance frequency (approximately 3.5 Hz). In this position, the electromagnetic coil was used in a simple absolute velocity feedback controller in an attempt to reduce the magnitude of the resonance peak. The gain of the feedback control was increased until the system became close to instability. Frequency response measurements over this range of feedback gains are shown in Fig. 8. Sampling parameters were as shown previously in Table 3.

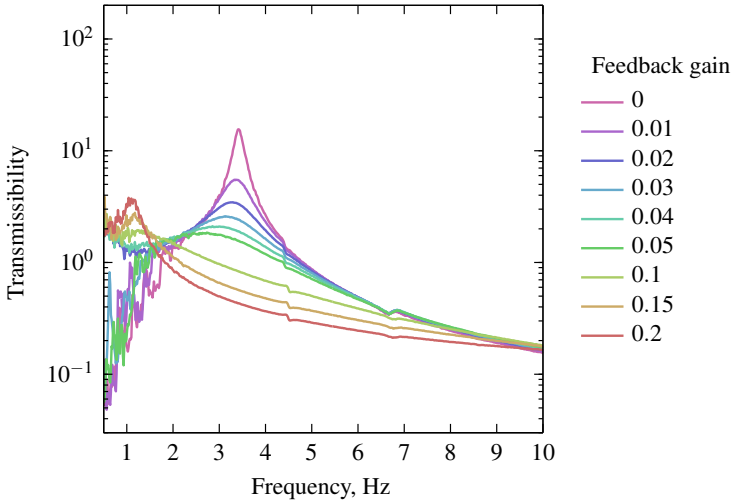

Figure 8. Closed loop frequency response measurements for a range of velocity feedback gains. The maximum feedback gain is close to instability for the system.

To estimate the velocity of the moving beam, the accelerometer measurement was integrated by the charge amplifier with a cut-on frequency of 1 Hz. Because the accelerometers were being used to measure velocity (via integrators in the charge amplifiers), the transmissibility curves shown in Fig. 8 were calculated from the ratio of the velocity measurements instead of acceleration measurements.

Due to the presence of higher-order dynamics in the structure, a low pass filter was used to reject signals above 50 Hz. This also ensured that aliasing was avoided when taking the frequency response measurements and when feeding back the velocity signal for the controller.

The overall improvement to the vibration isolation can be shown by calculating the root-mean-square of the transmissibility over a certain frequency range:

$$T_{\mathrm{RMS}} = \sqrt{\sum_{\omega=\omega_1}^{\omega_2} T(\omega)^2}. \tag{14}$$

The lower frequency limit is defined as $\omega_1 = 1$ Hz, as the results become very noisy below this frequency. The upper frequency limit $\omega_2 = 11$ Hz was chosen as the higher-order dynamics (not shown in Fig. 8) have little impact below this frequency.

Figure 9 shows the reduction in root-mean-square transmissibility T_{RMS} as the negative feedback gain increases. The overal transmissibility reduction is calculated as $1 - T_{\mathrm{RMS}}/T_0$, where T_0 is the root-mean-square transmissibility of the open loop system. The resonance at 1 Hz observed in Fig. 8 as the feedback gain increases causes the overall transmissibility reduction to have a local maximum.

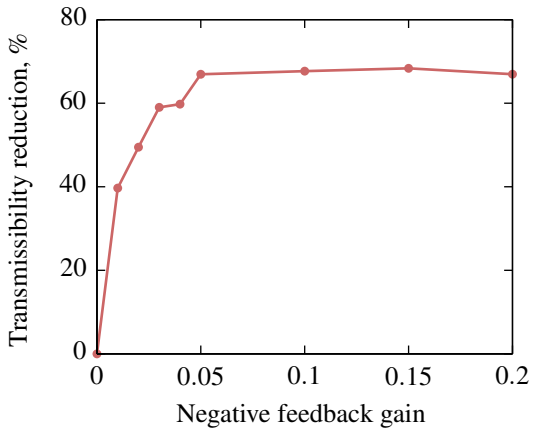

Figure 9. Affect on overall transmissiblity T_{RMS} between 1 Hz and 11 Hz as velocity feedback gain was increased.

Analysis of the gain-induced resonance

The appearance of a low frequency peak at 1 Hz in Fig. 8 as the feedback gain is increased is explained by the presence of the high-pass filter incorporated in the accelerometer charge amplifier, which also has a pole at 1 Hz. This behaviour has been shown previously for single degree of freedom structures with velocity feedback (Brennan, Ananthaganeshan, and Elliott 2007). Here, the same type of analysis will be used to investigate the response of a linear two degree of freedom isolator system (shown in Fig. 10) with integrated accelerometer measurements used for velocity feedback control.

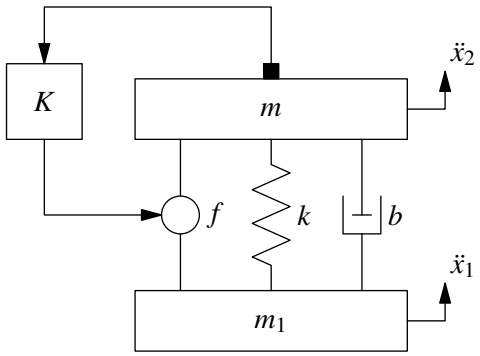

Figure 10. Vibration isolation schematic with active feedback.

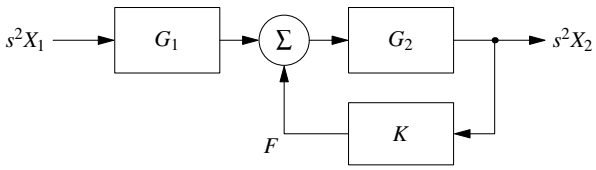

Figure 11. Block diagram of Eq. (16) representing the system shown in Fig. 10.

In the time domain, the response of this linear system is given by

$$m\ddot{x}_2 = f - b\left[\dot{x}_2 - \dot{x}_1\right] - k\left[x_2 - x_1\right], \tag{15}$$

which can be re-written in the Laplace domain as

$$s^2X_2\underbrace{\left[m + b/s + k/s^2\right]}_{[G_2]^{-1}} = F + s^2X_1\underbrace{\left[b/s + k/s^2\right]}_{G_1}. \tag{16}$$

This is shown as a block diagram in Fig. 11. If the control force is written as a function of the acceleration of the mass, $F = s^2X_2K$, the transmissibility of the system is

$$\frac{X_2}{X_1} = \frac{G_1G_2}{1 + KG_2}. \tag{17}$$

When the controller is some gain g_c in series with an ideal integration of the accelerometer signal, $K = g_c/s$, Eq. (17) simplifies to the idealised absolute velocity feedback expression:

$$\frac{X_2}{X_1} = \frac{k + bs}{k + \left[b + g_c\right]s + ms^2}. \tag{18}$$

This result is plotted in Fig. 12a for equivalent values of stiffness and damping as the experimental setup.

A more complex model for the controller block is required to account for the signal processing involved with amplifying and filtering the accelerometer signal to measure the velocity in reality. Assuming that the entire process between acceleration measurement and velocity output from the charge amplifier can be approximated as an ideal integrator in series with two high pass filters[3] (Brennan, Ananthaganeshan, and Elliott 2007), the controller block is defined as

$$K = \frac{g_c}{s}\left[\frac{s}{s + \omega_c}\right]^2, \tag{19}$$

where g_c is the absolute velocity feedback gain and ω_c is the corner frequency of the two high pass filters in the charge amplifier.

Using Eq. (19) in Eq. (17) gives the final transfer function between the mass and base states,

$$\frac{X_2}{X_1} = \frac{\left[bs + k\right]\left[s + \omega_c\right]^2}{g_cs^3 + \left[ms^2 + bs + k\right]\left[s + \omega_c\right]^2}. \tag{20}$$

This is plotted versus frequency in Fig. 12b, where the resonance induced by the high pass filter becomes apparent as the feedback gain is increased to 99% of the gain margin, which is the gain when the system becomes unstable. The simulation uses linear parameters $\omega = 3.5\,\mathrm{Hz}$ and $\zeta = 0.023$ in order to show results at similar behaviour to Fig. 8.

In order to calculate the gain margin of Eq. (20), KG_2 was evaluated equal to -1, where the system response of Eq. (17) becomes unbounded. To do this, first the critical frequency was found as the frequency at which $\mathrm{Im}(KG_2) = 0$; this frequency was then substituted into $\mathrm{Re}(KG_2) = -1$, which was solved for g_c to find the gain margin.

Comparing the simulated results of Fig. 12b with the experimental results of Fig. 8 shows a clear similarity between the two. The corner frequency of the high pass filter at 1 Hz in the charge amplifier to measure velocity is an impediment to the vibration isolation properties of the feedback-controlled system. This is a fundamental limitation in the use of accelerometers for estimating velocity for vibration control. To avoid this issue, the use of geophone sensors which measure velocity directly (such as used by Hong and Park (2010)) are a promising alternative to integrated accelerometer measurements. However, geophones are not a panacea since their response rolls off at low frequencies, limiting their performance at the frequency range of interest in this case.

[3] One filter for the integration of the acceleration signal, another for the conditioning electronics in the amplifier; assume for simplicity that they have the same cut-on frequency.

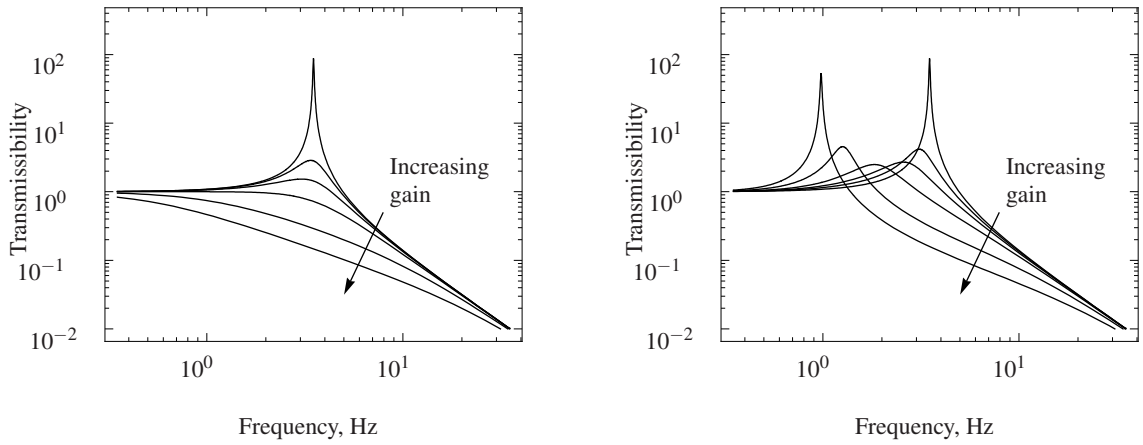

(a) Ideal velocity feedback.

(b) Integrated accelerometer feedback with a second order high pass filter.

Figure 12. Closed loop simulation with gains 0, 5, 10, 20, 50, and 99 percent of the gain margin in Fig. 12b.

CONCLUSION

In this paper, the experimental results have been presented from a magnetic system designed to demonstrate the ability of variable stiffness through position changes of the load-bearing magnets. As the system was brought closer to quasi–zero stiffness, the resonance frequency reduced until the operating point became too close to the position of marginal stability where even slight disturbances would yield instability. The minimum resonance frequency that could be achieved passively with this system was around 2 Hz. A lower resonance frequency than this could potentially be achieved with larger magnets with larger equilibrium magnet gaps, which would result in a larger physical region of stable operation near the quasi–zero stiffness position.

Without feedback control and without the actuator coil connected, the system showed very small damping ratios of around 0.005; these were dependent on the distance between the magnets at equilibrium. Connecting the non-contact electromagnetic actuator increased this damping ratio to around 0.03–0.04 due to eddy currents induced in the coils from the permanent magnet.

Dynamically, the system showed transmissibilities which could be modelled well by standard single degree of freedom models. With the very low damping of the open loop system, superharmonics were clearly visible in the variance gain but the resonance peaks remained linear-like. Once the actuator was connected, the additional eddy current damping suppressed these nonlinearities.

Absolute velocity feedback control was successful in reducing the transmissibility peaks, but as the gain was increased the additional poles added by the integration filters caused an additional lower frequency peak to appear as the closed loop system approached the gain margin. At best, the resonance peak was reduced by over an order of magnitude and the root mean square transmissibility was reduced by around 65%.

REFERENCES

Alabuzhev, P. et al. (1989). *Vibration Protecting and Measuring Systems with Quasi-Zero Stiffness*. Ed. by E. Rivin. Applications of Vibration. Hemisphere Publishing Corporation. ISBN: 0-89116-811-7.

Bassani, R. (Aug. 2006). "Earnshaw (1805—1888) and Passive Magnetic Levitation". *Meccanica* 41.4, pp. 375–389. DOI: 10.1007/s11012-005-4503-x.

Brennan, M. J., K. A. Ananthaganeshan, and S. J. Elliott (July 2007). "Instabilities due to instrumentation phase-lead and phase-lag in the feedback control of a simple vibrating system". *Journal of Sound and Vibration* 304.3–5, pp. 466–478. DOI: 10.1016/j.jsv.2007.01.046.

Carrella, A., M. J. Brennan, and T. P. Waters (Apr. 2007). "Static analysis of a passive vibration isolator with quasi-zero-stiffness characteristic". *Journal of Sound and Vibration* 301.3–5, pp. 678–689. DOI: 10.1016/j.jsv.2006.10.011.

Carrella, A. et al. (2008). "On the design of a high-static-low-dynamic stiffness isolator using linear mechanical springs and magnets". *Journal of Sound and Vibration* 315.3, pp. 712–720. DOI: 10.1016/j.jsv.2008.01.046.

Carrella, A. et al. (May 2009). "On the force transmissibility of a vibration isolator with quasi-zero-stiffness". *Journal of Sound and Vibration* 322.4–5, pp. 707–717. DOI: 10.1016/j.jsv.2008.11.034.

Cella, G. et al. (2005). "Monolithic geometric anti-spring blades". *Nuclear Instruments and Methods in Physics Research Section A: Accelerators, Spectrometers, Detectors and Associated Equipment* 540.2-3, pp. 502–519. DOI: 10.1016/j.nima.2004.10.042.

Chen, S.-L., J.-J. Liu, and H.-C. Lai (2009). "Wavelet analysis for identification of damping ratios and natural frequencies". *Journal of Sound and Vibration* 323.1-2, pp. 130–147. ISSN: 0022-460X. DOI: 10.1016/j.jsv.2009.01.029.

Hong, J. and K. Park (2010). "Design and control of six degree-of-freedom active vibration isolation table". *Review of Scientific Instruments* 81.3. DOI: 10.1063/1.3298605.

Jazar, G. N. et al. (2006). "Frequency Response and Jump Avoidance in a Nonlinear Passive Engine Mount". *Journal of Vibration and Control* 12, pp. 1205–1237. DOI: 10.1177/1077546306068059.

Lee, C.-M., V. N. Goverdovskiy, and A. I. Temnikov (May 2007). "Design of springs with "negative" stiffness to improve vehicle driver vibration isolation". *Journal of Sound and Vibration* 302.4–5, pp. 865–874. DOI: 10.1016/j.jsv.2006.12.024.

Molyneux, W. G. (1957). *Supports for vibration isolation*. ARC/CP-322. Aeronautical Research Council, Great Britain. URL: http://nsdl.org/resource/2200/20061003060308472T.

Robertson, W., B. Cazzolato, and A. Zander (July 2007). "Nonlinear control of a one axis magnetic spring". *Proceedings of the 14th International Congress on Sound and Vibration*. Cairns, Australia. ISBN: 978 0 7334 2516 5. URL: http://hdl.handle.net/2440/44996.

— (2011). "A simplified force equation for coaxial cylindrical magnets and thin coils". *IEEE Transactions on Magnetics* 47.8, pp. 2045–2049. DOI: 10.1109/TMAG.2011.2129524.

— (2012). "Axial force between a thick coil and a cylindrical permanent magnet: optimising the geometry of an electromagnetic actuator". *IEEE Transactions on Magnets* 48.9. DOI: 10.1109/TMAG.2012.2194789.

Robertson, W. et al. (2006). "Zero-stiffness magnetic springs for active vibration isolation". *Proceedings of the Sixth International Symposium on Active Noise and Vibration Control*. URL: http://hdl.handle.net/2440/35429.

Robertson, W. S. et al. (2009). "Theoretical design parameters for a quasi-zero stiffness magnetic spring for vibration isolation". *Journal of Sound and Vibration* 326.1–2, pp. 88–103. DOI: 10.1016/j.jsv.2009.04.015.

Tarnai, T. (Mar. 2003). "Zero stiffness elastic structures". *International Journal of Mechanical Sciences* 45.3, pp. 425–431. DOI: 10.1016/S0020-7403(03)00063-8.

Zhu, T. et al. (2011). "The development of a 6 degree of freedom quasi-zero stiffness maglev vibration isolator with adaptive-passive load support". *15th International Conference on Mechatronics Technology*. URL: http://hdl.handle.net/2440/72548.